Polymorphic behavior of 1,2-dipalmitoyl-3-lauroyl(PP12)- and 3-myristoyl(PP14)-*sn*-glycerols

Dharma R. Kodali, David Atkinson, and Donald M. Small

Department of Biophysics, Housman Medical Research Center, Boston University School of Medicine, 80 East Concord Street, Boston, MA 02118-2394

Abstract The polymorphic behavior and molecular packing in different polymorphic forms of stereospecific triacylglycerols, 1,2-dipalmitoyl-3-lauroyl-*sn*-glycerol (PP12) and 1,2-dipalmitoyl-3-myristoyl-*sn*-glycerol (PP14) were examined by X-ray diffraction, differential scanning calorimetry, infrared and Raman spectroscopy techniques. The molecular packing and the polymorphic behavior of the metastable forms of these two compounds are very similar. In both compounds the isotropic liquid, on quenching, crystallizes into a hexagonally packed α-phase. The long spacing periodicity of the α-phase indicates a tilted bilayer structure to compensate the voids created by the short acyl chains. Upon heating, the α-phase converts into an orthorhombic perpendicular ($O\perp$) β'_2-phase. The β'_2-phase, on further heating, exothermally converts to β'_1-phase with slightly different $O\perp$ subcell. On incubation of PP12 near the melting temperature of β'_1-phase, there is a slow (hours) conversion to a β-phase with triclinic parallel (T//) packing. However the β'_1-phase of PP14 is the most stable structure and the β-phase is absent. The thermodynamic parameters of the $O\perp$ packings of these compounds compared to those of the higher homologue, tripalmitoylglycerol, suggest that the $O\perp$ subcell is more stable in PP12 and PP14. The X-ray diffraction long spacings indicate that all the polymorphic forms of these compounds pack in a bilayer structure. The vibrational spectra confirm the lateral chain packing and inter- and intra-molecular order/disorder in the various polymorphic forms. The Raman and infrared spectra further indicate pertrubation in the carbonyl and the end methyl plane regions of the β'-phases.—**Kodali, D. R., D. Atkinson, and D. M. Small.** Polymorphic behavior of 1,2-dipalmitoyl-3-lauroyl(PP12)- and 3-myristoyl(PP14)-*sn*-glycerols. *J. Lipid Res.* 1990. **31:** 1853–1864.

Supplementary key words molecular packing • phase behavior • differential scanning calorimetry • X-ray diffraction • infrared and Raman spectroscopy

Triacyl-*sn*-glycerols are the major class of compounds of lipid storage in adipose tissue and take part in many biological processes. These long hydrocarbon chain compounds can pack in two or more crystalline modifications with similar lattice energy, called polymorphism (1). The physical properties of various polymorphic forms of an acylglycerol derivative, e.g., melting temperature, enthalpy, density and volume, differ from each other reflecting the differences in molecular packing (2). In triacylglycerols, packing along the molecular long and short axes is influenced by the nature of the acyl chain, i.e., length, unsaturation etc., and the position of esterification on the glycerol backbone. A knowledge of the molecular packing in different phases, and the temperature-induced intramolecular conformational changes that occur during their transformation from one polymorphic form to another, will enhance our understanding of polymorphism at the molecular level.

In triacylglycerols, based upon the lateral packing of the acyl chains, three common subcell structures, hexagonal, H (α-phase), orthorhombic perpendicular, $O\perp$ (β'-phase), and triclinic parallel, T// (β-phase) have been characterized (3). These forms can be distinguished from each other by X-ray wide-angle diffraction and infrared and Raman spectral data (1, 4, 5).

In the α-phase the adjacent acyl chain centers are separated from each other by about 4.85 Å in a two-dimensional hexagonal lattice without any specific chain–chain interactions. This type of acyl chain packing gives rise to a single strong wide-angle diffraction line at 1/4.2 $Å^{-1}$. In the β'-phase, the acyl chains are packed in an $O\perp$ subcell that gives rise to two or three intense wide-angle X-ray diffraction lines at 1/4.2 and 1/3.8 or 1/4.3, 1/4.1, and 1/3.8 $Å^{-1}$. This kind of packing can be identified in the infrared spectrum from the splitting of methylene rocking (720 cm^{-1}) and bending (1470 cm^{-1}) bands into two components due to intermolecular coupling of the methylene hydrogens of the adjacent acyl chains in the subcell (6–8). In the Raman spectrum this type of chain packing can be identified from a characteristic methylene

Abbreviations: DSC, differential scanning calorimetry; PP12, 1,2-dipalmitoyl-3-lauroyl-*sn*-glycerol; PP14, 1,2-dipalmitoyl-3-myristoyl-*sn*-glycerol.

scissoring band at 1420 cm^{-1} which is absent in the other two forms. The β-phase subcell is T//, where the zig-zag planes of the adjacent acyl chains are parallel to each other. This packing can be identified by its multiple X-ray diffraction wide-angle spacings with an intense line at $\sim 1/4.6$ $Å^{-1}$. In the infrared spectrum, in contrast to the β'-phase both α- and β-phases show sharp, strong absorptions for CH_2 bending and rocking modes without any split component (5, 9). Recently it has been shown that the Raman bands that occur in the 860–900 cm^{-1} are due to C_1 (carbonyl carbon)-C_2 (methylene carbon next to carbonyl) stretch of the acyl chains near the head group region and are sensitive to molecular packing order (10).

The molecular packing of simple saturated monoacid triacylglycerols trilaurin and tricaprin in the most stable polymorphic form (β-phase) has been determined by X-ray crystal structure analysis (11, 12). In these compounds the acyl chains esterified to the glycerol 1- and 2-hydroxyls point in opposite directions and the acyl chain at the 3-position bends at the carbonyl carbon region to lie parallel to the 1-acyl chain to give rise to a bilayer periodicity. A combination of saturated and unsaturated acyl chains substituted at different positions of glycerol and their effects on the molecular packing have been discussed (1) and reported (13–17).

The influence of acyl chain length on the molecular packing in the stable polymorphic forms of a homologous series of stereospecific 1,2-dipalmitoyl-3-acyl-*sn*-glycerols with a saturated 3-acyl chain of 2–16 carbons in length has been reported (15). Recently we reported the complex polymorphic behavior of 1,2-dipalmitoyl-3-decanoyl-*sn*-glycerol (PP10) (16). This compound showed five different polymorphic forms. The metastable forms, α, β'_3 and β'_2 packed in bilayered structures with variation in subcell packing. The stable forms, β'_1 and β packed in hexalayered and trilayered structures, respectively.

The overall thermal behavior and the comparison of molecular packing in general of this series have been reviewed (17). However, except for the studies of PP10 and PP16, the detailed molecular packing of different polymorphic forms has not been reported. This study reports the complex polymorphic behavior of 1,2-dipalmitoyl-3-lauroyl(PP12) and 3-myristoyl(PP14)-*sn*-glycerols after thermal treatment. The β' modifications that were identified in these compounds are designated by subscripts (β'_1, β'_2) with decreasing melting temperatures as suggested by Larsson (18).

MATERIALS AND METHODS

Optically active 1,2-dipalmitoyl-3-lauroyl and 3-myristoyl-*sn*-glycerols used in this study were synthesized according to the procedure described earlier (15). The purity of the compounds thus prepared was checked by TLC, HPLC, and elemental analysis (15).

Differential scanning calorimetry (DSC)

A Perkin-Elmer DSC-2 instrument (Norwalk, CT) was used over the temperature range of 5°C to 75°C and at a heating and cooling rate of 5°C/min, unless otherwise mentioned. Transition temperatures were determined as the position of the peak of transition. However, for the cooling scan, the onset of crystallization, i.e., the starting point for crystallization temperature, is also given. The base-lines (dotted lines in figures) were drawn connecting the flat base-lines of the beginning and the end of the transition peaks. Transition enthalpies were determined from the area under the peak and calibrated with a gallium standard. In this study the crystallization or melting of one phase is often overlapped by melting or crystallization of another phase. For such transformations we calculated the enthalpies by an indirect method. Since the enthalpy of crystallization of a phase is the same as that of melting, if we know the enthalpy of one transition (e.g., by crystallization from melt) then, using the partial enthalpies of melting and recrystallization, we can calculate the enthalpies of the overlapping transitions.

X-ray diffraction

Diffraction patterns were recorded on photographic films. Nickel-filtered CuKα radiation (λ = 1.5418 Å) from a rotating anode Elliot GX6 (Marconi Avionics, Hertfordshire, England) X-ray generator was collimated by Elliot torroidal mirror optics or Frank's double mirror optics (19). The samples were packed in thin-walled quartz capillary tubes (diameter 1 mm, Charles Supper Co., Inc., Natick, MA). The samples were mounted in a variable temperature sample holder with a temperature accuracy of $\pm$ 1–2°C.

Vibrational spectroscopy

Infrared spectra were recorded by using a Perkin-Elmer 1310 double-beam infrared spectrophotometer. The compound in the form of KBr pellet was placed between KBr windows in a variable temperature cell (Harrick Scientific Corporation, Ossining, NY). Care was taken during the pellet making not to use excessive pressure to avoid phase transformation of the compound. Raman spectra were recorded with a Spex Raman spectrophotometer equipped with a double monochromator and a photomultiplier. The 5145 Å line from an Innova 70 argon ion laser (Coherent Laser Products, Palo Alto, CA) with a power of 75–200 mW at the sample was used as the excitation source. Spectral frequencies are calibrated with laser plasma lines. Raman spectra were recorded at a scanning rate of 27 cm^{-1}/min with a spectral resolution of ~ 5 cm^{-1}. The powder sample packed in a capillary tube was placed in the Harney-Miller variable temperature assembly and the scattered radiation at the right angle was measured. The temperature was monitored by a thermocouple introduced in the exit end of the Harney-Miller cell, close to the sample.

RESULTS

PP12

β-Phase. The compound crystallized from hexane at room temperature melted to an isotropic liquid at 56.1°C with an enthalpy of fusion of 32.3 kcal/mol (**Fig. 1a**). The

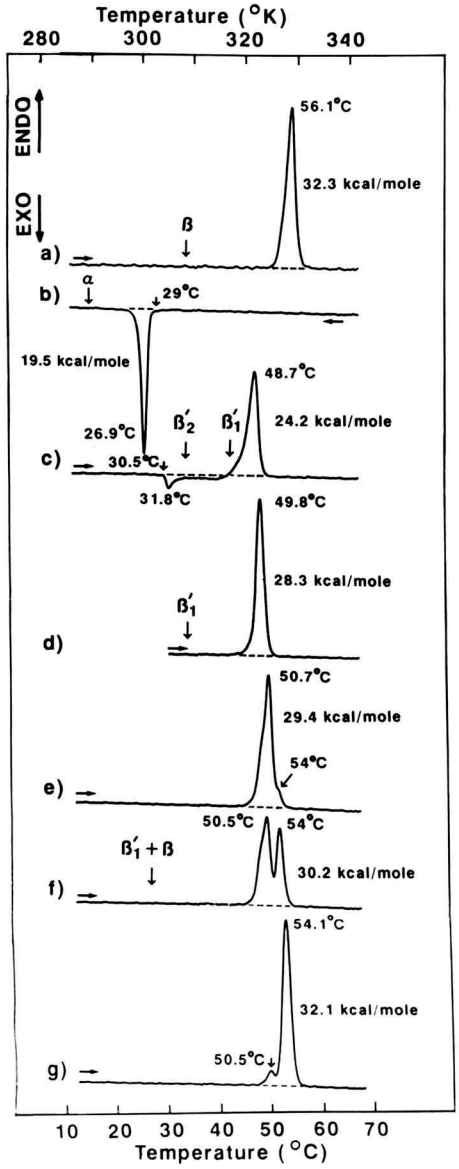

Fig. 1. Thermal behavior of PP12. The horizontal arrows indicate heating→; and cooling←scans. The various polymorphic forms identified by the X-ray diffraction and vibrational spectroscopy are indicated in Greek letters on the DSC curves at appropriate places with vertical arrows. a) First heating scan showing the melting of β-phase obtained from solvent of crystallization. b) Cooling scan showing the crystallization of isotropic liquid into α-phase. c) Immediate reheating shows the conversion of α-phase into β'_2-phase, and the subsequent exothermal transformation into β'_1-phase. d) The melting transition of β'_1-phase on heating, which was obtained from the α-phase by heating to 47°C and on incubation at this temperature for 10 min and cooling to 27°C. The conversion of β'_1-phase to β-phase is shown after incubating the β'_1-phase at 44°C for e) 2.5 h, f) 4 h, and g) 14.5 h.

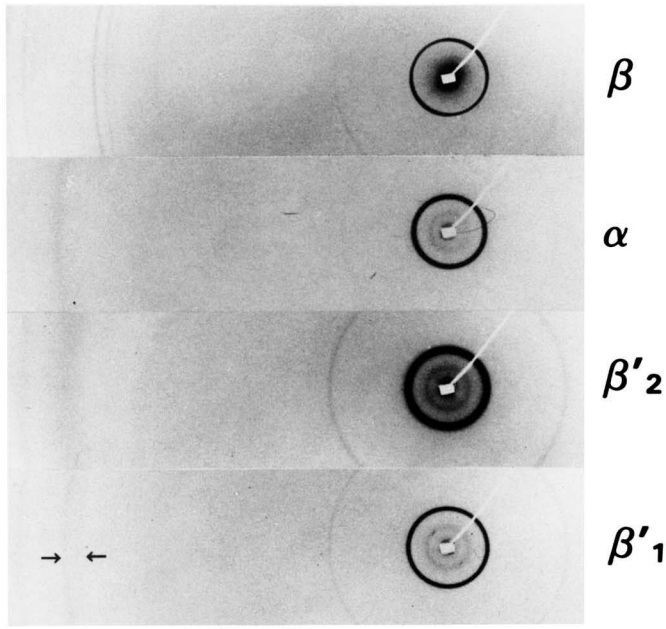

Fig. 2. X-ray diffraction pattern of β, α, β'_2, and β'_1-phases of PP12. The inner diffuse line in the α, β'_2 and β'_1 and β-phases which occurs at 1/75 $Å^{-1}$ is an artifact arising from the backstop. The diffraction is recorded with Frank's optics with a sample to detector distance of 220 mm.

X-ray diffraction pattern of this phase was typical of a β-phase as shown in **Fig. 2**. The low angle region showed three (001) reflections that index to a periodicity of 41 Å. The wide-angle region showed multiple lines with intense diffraction line at 1/4.57 $Å^{-1}$ characteristic of T// packing. The thermodynamic parameters are given in **Table 1** and the X-ray diffraction spacings with the intensities of this phase are listed in **Table 2**. The infrared spectrum of this phase (**Fig. 3a**) showed strong and sharp methylene scissoring (1469 cm^{-1}) and rocking (718 cm^{-1}) absorption bands with band widths of 10 and 7.5 cm^{-1} at half-peak height, respectively. The symmetric methyl deformation band appeared at 1389 cm^{-1}. The carbonyl absorption of the ester linkage is symmetrical at 1735 cm^{-1}. **Fig. 4d** shows the Raman spectrum of this phase, and the various Raman band frequencies along with the intensities are given in **Table 3**.

α-Phase. On cooling the isotropic liquid, the α-phase crystallized at 26.9°C with an enthalpy of crystallization of 19.5 kcal/mol (Fig. 1b). The wide-angle X-ray diffraction showed a single strong diffraction at 1/4.14 $Å^{-1}$ characteristic of hexagonal subcell. The long spacing of this phase is 43.3 Å (Fig. 2). The α-phase on heating exothermally converts to a β'_2-phase at 31.8°C. However the melting of α-phase at 32°C can be observed before it transforms into β'_2-phase, if the isotropic liquid is cooled rapidly (20°C/min) to 7°C and then immediately reheated at 10°C/min (data not shown). The thermodynamic data and the X-ray diffraction information of

TABLE 1. Thermodynamic data of various phases of PP12 and PP14

Phase	Compound	T_m (°C)[a]	ΔH[b]	ΔS[c]	T_c (°C)[d]
			kcal/mol	*Cal · mol⁻¹ · K°⁻¹*	
β-Phase	PP12	56.1	32.3[e]	98.1	[f]
β'_1-Phase	PP14	58.6	34.0[e]	102.5	43[g]
β'_1-Phase	PP12	49.8[h]	28.3[h]	87.7	41.5[g] (39.1)
β'_2-Phase	PP14	[f]	26.5[i]	[j]	40.5
β'_2-Phase	PP12	[f]	22.5[i]	[j]	31.8 (30.5)
α-Phase	PP14	39.5	22.3[k]	71.4	35.5 (36.7)
α-Phase	PP12	32.0[l]	19.5[k]	63.9	26.9 (29.0)

[a]Temperature of melting, transition peak values.
[b]Enthalpy of melting transition.
[c]Entropy of melting transition, calculated from the enthalpy of melting.
[d]Temperature of crystallization, transition peak values. The values in the parentheses are the onset of crystallization temperatures.
[e]These values are for the forms obtained from solvent of crystallization.
[f]These transitions are not observed as they form upon incubation of solids.
[g]These transitions are broad and the values are taken from the mid-point.
[h]These values are obtained after incubating the β'_1-phase formed from α-phase, at 47°C for 10 min.
[i]Calculated from the crystallization enthalpies of α-phase and β'_2-phase.
[j]Due to lack of melting transition temperatures (these transitions occur solid to solid) the entropies were not determined.
[k]These values are taken from the enthalpies of crystallization.
[l]This value is obtained after cooling the melt at 20°C/min and on immediate reheating at 10°C/min.

this phase are listed in Tables 1 and 2, respectively. The infrared spectrum of this phase (Fig. 3b) shows narrow methylene scissoring and rocking bands at 1468 and 721 cm^{-1} with band widths of 8 and 11 cm^{-1} at half the peak heights, respectively. The ester carbonyl and methyl deformation absorptions are observed at 1738 and 1378 cm^{-1}, respectively, without any split component. The Raman spectrum of this phase is shown in Fig. 4a and the band frequencies with the intensities are given in Table 3.

β'_2-Phase. On heating, the α-phase transformed into β'_2-phase at 31.8°C (exothermic peak in Fig 1c). The enthalpy of fusion of the β'_2 phase, 22.5 kcal/mol, is calculated by an indirect method, by adding the enthalpy of crystallization of β'_2-phase (Fig. 1c) to the enthalpy of crystallization of α-phase from the melt (Fig. 1b). The X-ray diffraction pattern of this phase is obtained after heating the α-phase to 32°C, holding at this temperature for 3 min, and then recording the X-ray diffraction at 3°C (Fig. 2). The wide-angle region showed two diffraction lines at 1/4.25 and 1/3.84 $Å^{-1}$, characteristic of an O⊥ subcell. The diffraction line at 1/4.25 $Å^{-1}$ is very broad from 1/4.34 to 1/4.16 $Å^{-1}$. The long spacings of this phase index to 39 Å. The X-ray diffraction data is listed in Table 2. On further heating this phase converts exothermally to β'_1-phase. The infrared spectrum of this phase (Fig. 3c) showed relatively broad bands at 1470 and 721–730 cm^{-1} with band widths of 14 and 16 cm^{-1} measured at half the height, respectively. The methyl deformation band is split into two bands at 1380 and 1391 cm^{-1}. The carbonyl stretching band of the ester also showed splitting into 1740 and 1728 cm^{-1}. The Raman spectrum of this phase is shown in Fig. 4b and the frequencies and the intensities of various bands are listed in Table 3.

TABLE 2. X-ray diffraction long and short spacings with intensities of PP12 and PP14[a]

Phase	Compound	Long Spacings (Å)			Short Spacings (Å)
β-Phase	PP12	40.9 (S)	20.5 (VW)	13.70 (M)	5.47 (M), 4.71 (M), 4.57 (S), 3.90 (M), 3.74 (S)
β'_1-Phase	PP14	40.5 (S)		13.4 (M)	4.36 (M), 4.19 (S), 3.99 (W), 3.80 (S)
β'_1-Phase	PP12	39.0 (S)		13.10 (M)	4.39 (M), 4.23 (S), 4.03 (W), 3.83 (S)
β'_2-Phase	PP14	40.4 (S)		13.44 (W)	4.21 (S)[b], 3.80 (W)
β'_2-Phase	PP12	39.0 (S)		13.11 (W)	4.25 (S)[b], 3.84 (M)
α-Phase	PP14	45.3 (S)		15.0 (W)	4.13 (S)
α-Phase	PP12	43.3 (S)		14.43 (W)	4.14 (S)

[a]The relative intensities are shown in parentheses, S, strong; M, medium; W, weak.
[b]These diffraction lines are broad.

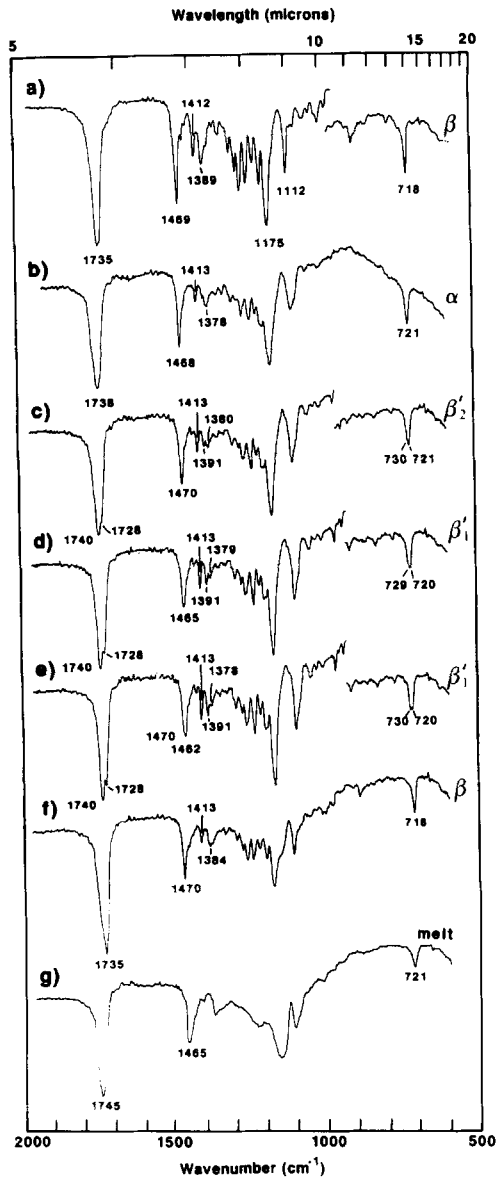

Fig. 3. Infrared spectra of various polymorphic forms of PP12. The spectrum of each phase is identified by a Greek letter. a) β-Phase crystallized from hexane, the spectrum is recorded at 20°C; b) α-phase, obtained after quenching the isotropic liquid and the spectrum is recorded at 3°C; c) β'_2-phase, the spectrum is recorded at 35°C; d) β'_1-phase, the spectrum is recorded at 47°C; e) annealed β'_1-phase obtained after incubating the β'_1-phase at 30°C for 15 h and the spectrum is recorded at 30°C; f) β-phase, obtained after heating the previous annealed β'_1-phase to 52.5°C, the spectrum is recorded at 52.5°C; g) liquid, obtained after heating to 70°C and the spectrum is recorded at 59°C. All the spectra were recorded from a single KBr pellet, in the sequence of a, g, b, c, d, e, f.

β'_1-Phase. This phase transformed from β'_2-phase exothermally at 41.5°C and on further heating melted at 48.7°C to an isotropic liquid with an enthalpy of fusion of 24.2 kcal/mol (Fig. 1c). As the crystallization and melting temperatures are close, to allow the complete formation of β'_1-phase, the α-phase obtained after cooling is heated to 47°C and incubated at this temperature for 10 min and then cooled. The subsequent heating gave an enthalpy of 28.3 kcal/mol and a melting temperature of 49.8°C (Fig. 1d). The X-ray diffraction pattern, obtained after heating the α-phase to 44°C (holding at this temperature for 3 min) and then recording the diffraction experiment at 3°C, gave wide-angle diffraction lines at 1/4.39, 1/4.23, 1/4.03, and 1/3.83 $Å^{-1}$ (Fig. 2). The broad diffraction lines at 1/4.25 of β'_2-phase is replaced by two sharp lines at 1/4.39 and 1/4.23 $Å^{-1}$. The long spacing of this phase is 1/39 $Å^{-1}$, same as that of β'_2-phase. The β'_1-phase

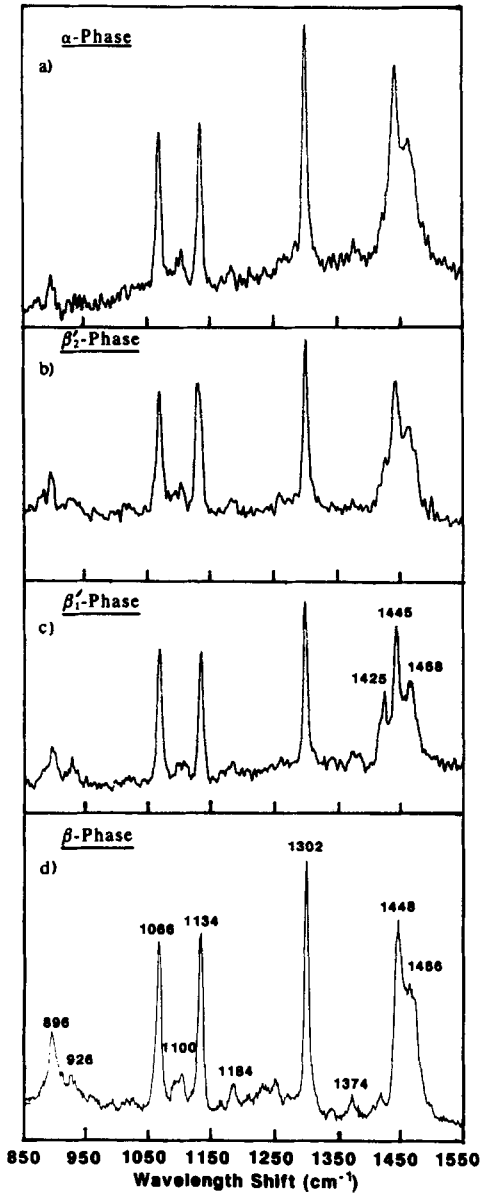

Fig. 4. Raman spectra of various polymorphic forms of PP12. a) α-Phase obtained after quenching the liquid to − 10°C and the spectrum is recorded at − 10°C; b) β'_2-phase obtained after incubating the α-phase at 32.5°C for 3 min and the spectrum is scanned at − 10°C; c) β'_1-phase obtained after incubating the β'_2-phase at 44°C for 3 min and the spectrum is recorded at − 10°C; d) β-phase obtained from solvent of crystallization, recorded at 15°C.

TABLE 3. Raman band frequencies and intensities of various polymorphic forms of PP12 and PP14[a]

Polymorphic Form	Compound	Raman Band Frequencies cm^{-1} (intensity)													
β-Phase	PP12	880 (6)	896 (27)	927 (11)	1066 (65)	1100 (13)	1134 (69)	1302 (100)	1420 (10)	1448 (78)	1466 (53)	2852 (77)	2887 (133)	2937 (35)	2965 (23)
β'_1-Phase	PP14	880 (10)	895 (25)	926 (16)	1067 (78)	1103 (17)	1133 (74)	1301 (100)	1425 (42)	1446 (82)	1465 (53)	2852 (75)	2887 (132)	2938 (29)	2963 (19)
β'_1-Phase	PP12	879 (11)	895 (25)	927 (19)	1068 (79)	1097 (17)	1134 (74)	1300 (100)	1425 (44)	1445 (83)	1468 (52)	2852 (80)	2886 (127)	2935 (35)	2964 (21)
β'_2-Phase	PP14	875 (7)	892 (19)	924 (8)	1064 (74)	1097 (16)	1130 (74)	1297 (100)	1421 (29)	1440 (76)	1463 (50)	2848 (66)	2883 (117)	2938 (31)	2963 (16)
β'_2-Phase	PP12	880 (13)	894 (28)	928 (13)	1068 (73)	1102 (19)	1129 (75)	1300 (100)	1426 (34)	1443 (76)	1463 (53)	2852 (84)	2886 (140)	2935 (40)	2964 (21)
α-Phase	PP14	877 (9)	892 (22)	[b]	1064 (68)	1098 (19)	1130 (75)	1296 (100)	[b]	1439 (75)	1462 (46)	2848 (66)	2883 (93)	2938 (28)	2963 (14)
α-Phase	PP12	875 (7)	894 (15)	[b]	1067 (66)	1103 (18)	1133 (68)	1300 (100)	1422 (22)	1443 (82)	1464 (53)	2851 (67)	2888 (96)	2935 (29)	2965 (19)

[a]The intensities are measured as peak heights from the baseline and normalized by taking 1300 cm^{-1} as 100.
[b]These bands are absent.

is stable at low temperatures. However, when incubated near its melting temperature, the β-phase nucleates and grows at the expense of β'_1-phase. This transformation of the β'_1-phase into the β-phase upon incubation at 44°C is shown in Fig. 1e, f, and g. The infrared spectrum of β'_1-phase (Fig. 3d) showed broad methylene scissoring and rocking bands at 1465 and ~725 cm^{-1} with band widths of 17 and 16 cm^{-1}, respectively. The carbonyl stretching absorption and methyl deformation bands are split. After annealing this phase (held at 30°C for 15 h) the splitting of the carbonyl stretching, methylene scissoring, and methyl deformation bands are more pronounced (Fig. 3e). The Raman spectrum of this phase (Fig. 4c) shows methylene scissoring band at 1425 cm^{-1} characteristic of O⊥ packing. The various Raman band frequencies along with their intensities are reported in Table 3.

PP14

β'_1-Phase. This compound on crystallization from hexane gave a β'_1-phase. The melting temperature and the enthalpy of fusion are 58.6°C and 34.0 kcal/mol, respectively (**Fig. 5a**). The X-ray diffraction pattern of this phase showed 40.5 Å long spacing and wide-angle diffraction at 1/4.36, 1/4.19, 1/3.99, and 1/3.80 $Å^{-1}$ (Table 2). The wide-angle diffraction lines are characteristic of O⊥ packing. The infrared spectrum (**Fig. 6a**) of this phase shows broad methylene scissoring at 1462 cm^{-1} and methylene rocking at 720–730 cm^{-1}. Even though the splitting of these bands is not conspicuous, the peak widths measured at half-peak height are 20 cm^{-1} and 17.5 cm^{-1}, respectively. The carbonyl stretching (1739 and 1727 cm^{-1}) and methyl deformation (1391 and 1378 cm^{-1}) showed clear splitting into two components. The Raman spectrum (**Fig. 7c**) of this phase shows a strong band at 1425 cm^{-1} characteristic of O⊥ packing. The β'_1-phase is the most stable form and melts to an isotropic liquid on heating. Attempts to nucleate a β-phase at different temperatures or from solvent of crystallization failed.

α-Phase. On cooling the isotropic liquid, the α-phase crystallizes at 35.5°C with an enthalpy of crystallization of 22.3 kcal/mol (Fig. 5b). The X-ray diffraction of this phase gave a long spacing of 45.3 Å. A single strong wide angle diffraction line at 1/4.13 $Å^{-1}$ is characteristic of hexagonal packing. The infrared spectrum of this phase (Fig. 6b) shows sharp bands for methylene scissoring (1466 cm^{-1}) and rocking (721 cm^{-1}). The peak widths of these bands measured at half-peak height are 10 cm^{-1} each. The α-phase on heating, melts at 39.5°C and converts to β'_2-phase.

β'_2-Phase. The α-phase transformed into β'_2-phase at 40.5°C. The enthalpy of this phase calculated indirectly from the enthalpy of crystallizations of α-phase from melt and β'_2-phase from α-phase is 26.5 kcal/mol. The X-ray diffraction pattern of this phase gave a long spacing value of 40.4 Å. The wide-angle diffraction lines at 1/4.21 and 1/3.80 $Å^{-1}$ indicate the O⊥ packing (Table 2). The infrared spectrum (Fig. 6c) shows broad bands for methylene scissoring at 1465 cm^{-1} (17.5 cm^{-1} wide at half-peak height) and methylene rocking at 720–730 cm^{-1} (15 cm^{-1} wide at half-peak height). The symmetric methyl deformation split into two components of equal intensity at 1391 and 1379 cm^{-1}. The Raman spectrum (Fig. 7b) showed 1421 cm^{-1} band confirming the O⊥ subcell. The β'_2-phase upon further heating exothermally converts to β'_1-phase. The β'_1-phase thus obtained melted at 56.0°C with an enthalpy of melting of 29 kcal/mol (Fig. 5c). Upon incubation of β'_1-phase at 51.5°C for different lengths of time (Fig. 5d, e, and f), increased the enthalpy

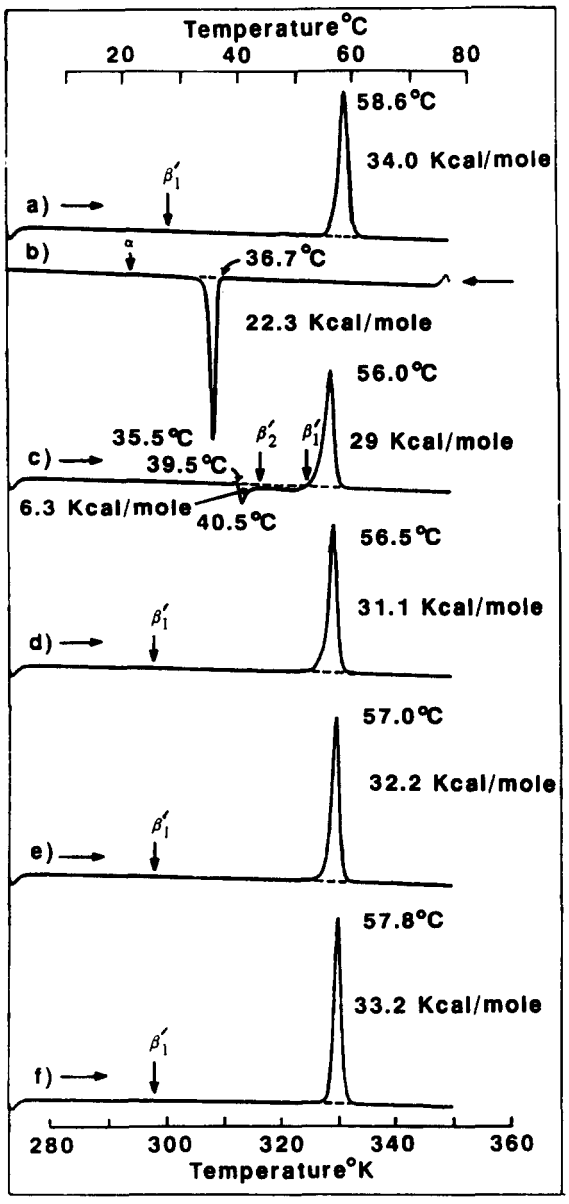

Fig. 5. Thermal behavior of PP14. The horizontal arrows indicate heating→; and cooling←scans. The various polymorphic forms identified by the X-ray diffraction and vibrational spectroscopy are shown in Greek letters on the DSC traces at appropriate places with vertical arrows. a) First heating scan showing the melting of β'_1-phase obtained from solvent of crystallization; b) cooling scan showing the crystallization of isotropic liquid into α-phase; c) immediate reheating shows the α-phase transformation into β'_2-phase, which on further heating exothermally converts into β'_1-phase; d) the melting of β'_1-phase which was obtained after heating the α-phase to 51.5°C and on cooling. The melting transition of β'_1-phase after it is incubated at 51.5°C for e) 20 min, and f) 70 h.

and melting temperature close to those of the form obtained from solvent or crystallization. In spite of prolonged incubated (70 h) the β'_1-phase does not nucleate the β-phase (Fig. 5f).

DISCUSSION

The molecular packing of the most stable polymorphic forms of PP12 and PP14 are different. The PP12 crystallized from solution packed in T// subcell, whereas PP14 packed in O⊥ subcell. Using thermal manipulation we were able to isolate and identify the other metastable forms in these compounds. The stability, thermodynamic parameters, and the packing in terms of subcell structure and the repetition periodicity are compared with the

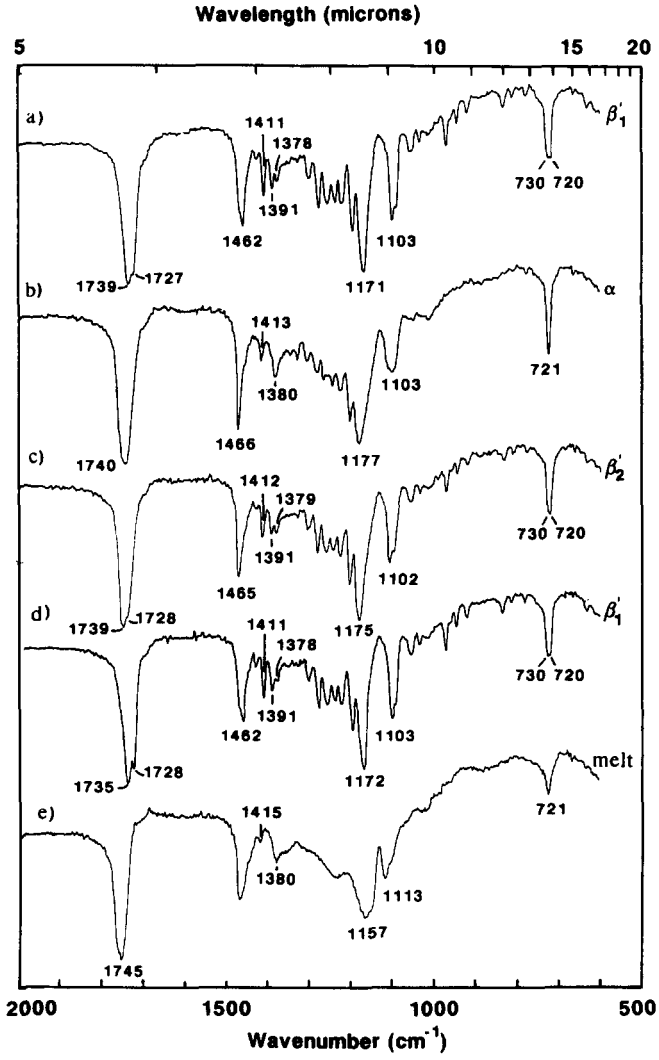

Fig. 6. Infrared spectra of various polymorphic forms of PP14. The spectrum of each phase is identified by a Greek letter. a) β'_1-Phase crystallized from hexane, the spectrum is recorded at 20°C; b) α-phase obtained after quenching the isotropic liquid and the spectrum is recorded at 10°C; c) β'_2-phase obtained after heating the α-phase to 45°C and held at 45°C for 3 min and the spectrum is recorded at 30°C; d) annealed β'_1-phase obtained after heating the β'_2-phase to 52°C for 30 min and the spectrum is recorded at 52°C; e) liquid, obtained after melting the compound by heating to 64°C and the spectrum is recorded at 64°C. All the spectra were recorded from a single KBr pellet in the sequence of a, e, b, c, d.

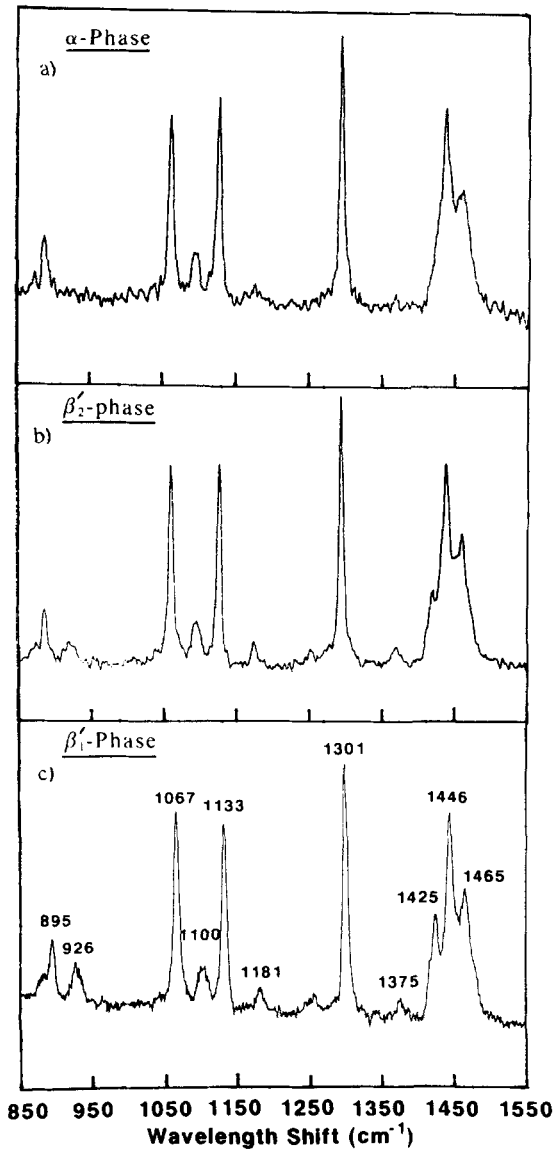

Fig. 7. Raman spectra of various polymorphic forms of PP14. a) α-Phase obtained after quenching the liquid to −4°C and is recorded at −4°C; b) β'_2-phase obtained after incubating the α-phase at 41°C for 3 min and the spectrum at −3°C; c) β'_1-phase crystallized from hexane and the spectrum is recorded at 15°C.

higher homologue of the series tripalmitoylglycerol (PP16).

Carter and Malkin (20, 21) examined the phase behavior of racemic compounds. Melting temperatures of the highest melting polymorph reported for these two compounds (PP12, β-phase 54°C; PP14, β-phase 57°C) are lower than the ones found in this study indicating that the fatty acids used and the final compounds were not pure. In addition, at that time (1939), there was considerable confusion regarding the nomenclature of the metastable forms and it is obviously very difficult to compare these results (22). We believe that the differences in the thermodynamic data and the X-ray diffraction long spacings given by Carter and Malkin and this study could be due to either the racemic mixture or the purity of fatty acids or both.

Stability and interconversion

On cooling from the isotropic liquid, an hexagonally packed α-phase is crystallized in both PP12 and PP14. The α-phase is the least stable metastable form of these compounds. The enthalpies (expressed in kcal/-CH_2- to correct for a different number of methylenes) of α-phase are 0.51 and 0.56 for PP12 and PP14, respectively, both lower than that of tripalmitoylglycerol [0.59 kcal/-CH_2-(22)] but higher than PP10 [0.42 kcal-CH_2-(16)]. The entropies of transformation of this phase show a similar trend with the values of 1.40, 1.68, 1.79, and 1.92 cal/-CH_2-/°K for PP10, PP12, PP14, and PP16, respectively. The long spacings of the α-phase of PP10 (40.4 Å) (16), PP12 (43.3 Å), and PP14 (45.3 Å) are shorter than that of PP16 (45.8 Å) (23). The difference between the experimental and theoretical long spacing values provide information on the acyl chain tilt. In PP16 the acyl chains are perpendicular to the layer plane, but the bilayer structures of PP14, PP12, and PP10 are increasingly tilted from the basal methyl plane. In PP10 and PP12 where the long spacings are much shorter, in addition to the tilt, there is a possibility of conformational disordering in the methyl end region where the short acyl chains leave vacant spaces that can effectively reduce the long spacings. In these compounds the melting temperatures of α-phase increased with the molecular weight. The stability of α-phase below its melting temperature decreased in the order of PP16 > PP14 > PP12. This may indicate that the chain inclination or disordering more readily forces the conversion of α-phase into β'_2-phase.

Either on prolonged incubation or on heating, the α-phase converts to β'_2-phase. The $\alpha \rightarrow \beta'_2$ transition is melt-promoted but can be a solid-to-solid transformation if held for longer time at temperatures below the α-phase melting temperature. The enthalpy of fusion values for β'_2-phase of PP12 and PP14 were found to be 0.59 and 0.66 kcal/-CH_2-, respectively. Both these values are greater than that of PP16 (0.53 kcal/-CH_2-) (24), indicating higher stability of this phase in PP12 and PP14. The long spacings of β'_2-phase indicate a greater tilt from the basal plane than the corresponding α-phase. The metastable β'_2-phase has stability intermediate between α- and β'_1-phases. The $\beta'_2 \rightarrow \beta'_1$ conversion is continuous at the heating rate of 5°C/min (Figs. 1c and 5c); however, the β'_2-phase can be isolated and stabilized by cooling immediately after its formation.

The enthalpy of fusion and melting temperature of β'_1-phase of PP12, obtained after $\beta'_2 \rightarrow \beta'_1$ conversion are 24.2 kcal/mol and 48.7°C, respectively. Both these values in-

creased after incubating the β'_1-phase at 47°C for 10 min (Fig. 1d) to 28.3 kcal/mol and 49.8°C, respectively. Similarly, in PP14 the enthalpy of fusion and melting temperatures of β'_1-phase immediately after its formation from β'_2-phase (Fig. 5c) are lower than that obtained from solvent of crystallization (Fig. 1a). Incubation at 51.5°C (Fig. 5e and f) showed considerable increase in the melting temperature and enthalpy of fusion. After the incubation at 51.5°C for 70 h, the difference in melting temperature and enthalpy of fusion between the incubated (Fig. 5f) and solvent crystallized (Fig. 5a) forms is very small (0.8°C and 0.8 kcal/mol, respectively). The difference in melting temperature and enthalpy of fusion of the same phase obtained by different procedures may be due to differences in crystal size and perfection. In spite of the thermodynamic differences there is no observable difference in the X-ray diffraction pattern of this phase.

The enthalpy of fusion values of the stabilized β'_1-phase for PP12 and PP14 are 0.74 and 0.85 kcal/-CH_2-. The corresponding value of tripalmitoylglycerol (0.75 kcal/-CH_2-) (22) is similar to that PP12. The gains in entropy after this transition for PP12, PP14, and PP16 are 2.29, 2.56, and 2.27 cal/-CH_2-/°K, respectively. The greater change in enthalpy and entropy of melting values of the β'_1-phase of PP14 indicate that the Gibbs free energy of this phase is less for PP14 than for PP12 and PP16. The β-phase enthalpy of fusion values of PP12 and PP16 are 0.85 and 0.95 kcal/-CH_2-, respectively. If PP14 were to form a β-phase, the enthalpy of fusion would have been intermediate, i.e., about 0.90 kcal/-CH_2-. Then the difference in enthalpy of fusion between β'_1 and β would have been only 0.05 kcal/-CH_2-. This minimal difference between the packing energies of β'_1, and β-phases is probably partially responsible for the absence of β-phase in PP14.

Recently Hernquist (25) concluded that the $\beta' \rightarrow \beta$ transition is delayed or hindered by stabilization of the orthorhombic chain packing. He suggested that stabilization of O⊥ packing can arise from the dissimilarity in the acyl chain lengths resulting in an inter-chain-penetrated region between the stacks of layers that prohibit the formation of β-phase. If this is true, the formation of β-phase would have been hindered more in PP12 rather than in PP14. As this is not the case, there might be other structural and or thermodynamic reasons as noted above. From the X-ray wide-angle diffraction lines it appears that the lateral chain packing of the β'_1-phase in both PP12 and PP14 is very similar, and like that in the analogous phase of PP10 (16). The most stable polymorphic form of diacid triacylglycerols of type $C_{16}C_{17}C_{16}$ and $C_{18}C_{19}C_{18}$ pack in β'-phase and the β-phase is absent (22), indicating that the packing in the methyl end region can influence the formation of β-phase. Therefore, the extra stability of β'_1-phase of PP14 and its inability to form β-phase probably arise from the end group methyl packing and the interlamellar packing between the stacks of bilayers.

Subcell structure

The hexagonal packing in the α-phase of both PP12 and PP14 is evident from the wide-angle diffraction and is consistent with the strong and sharp CH_2 bending and rocking bands at ~1470 and ~720 cm^{-1} (Figs. 3b and 6b). The O⊥ packing in the β'_2-phase of these two compounds are similar as they produce similar wide-angle diffraction lines. However, the broad 1/4.2 $Å^{-1}$ diffraction line indicates that this diffracting plane is probably somewhat variable. In the wide-angle region of the β'_1-phase of both PP12 and PP14, the broad 1/4.2 $Å^{-1}$ diffraction line of β'_2-phase is replaced by two sharp lines at ~1/4.3 and 1/4.2 $Å^{-1}$. This observation is in agreement with our previous findings (16) and of others (26). The infrared spectra of both β'_1 and β'_2 showed broad methylene bending and rocking bands and the insufficient spectral resolution does not allow us to separate the two components present in these bands. The Raman spectra of the β'_1 and β'_2-phases showed a ~1420 cm^{-1} peak, associated with a split component of the Raman-active methylene scissoring mode, characteristic of a O⊥ packed hydrocarbon chains (5).

The following are some of the general characteristic features that are observed in the vibrational spectra of different polymorphic forms. In general, the band widths measured at half-peak height, for methylene rocking (~720 cm^{-1}) and bending (~1470 cm^{-1}) bands of O⊥ forms are broader (14–20 cm^{-1}) than the hexagonal and T// forms (8–11 cm^{-1}). As observed earlier the infrared spectra of the carbonyl band of the O⊥ packed forms showed a clear splitting into low and high frequency bands at 1725 and 1740 cm^{-1} (16). This suggests that two different conformations exist around the carbonyl region. Bicknell-Brown, Brown, and Person (27) have observed two carbonyl stretching bands at 1740 and 1720 cm^{-1} in the Raman spectra of anhydrous crystalline phosphoglycerides. The high frequency band arose from the *gauche* conformation and the lower frequency band is due to *trans* conformation at the carbonyl carbon and the carbon next to it (C_1–C_2 carbon-carbon bond). The infrared spectra of the β'-forms show the intensity ratio of 1740 to 1725 cm^{-1} is 2:1. From this one can assume that for each molecule two acyl linkages at the C_1–C_2 are *gauche* and one is *trans*. The splitting of the C=0 absorption increased from β'_2 to β'_1. In the annealed β'_1-spectrum (Figs. 3e and 6d) this splitting is more pronounced. In the O⊥ packed β'-phases the symmetric methyl deformation mode is split into ~1380 and 1390 cm^{-1} peaks. In the β'_2-phase both these frequencies are of equal intensity and in the β'_1-phase the band at the higher frequency is stronger. There-

fore, the differences in packing between the two β'-phases arise in the carbonyl region and the end methyl region.

The principal bands in the C-H stretching region (2800-2950 cm^{-1}) are methylene symmetric stretch (2850 cm^{-1}) and asymmetric stretch (2885 cm^{-1}), and methyl C-H stretch (2935 cm^{-1}). As pointed out by Larsson the β-phase of PP12 shows a band at 2865 cm^{-1} characteristic of T// packed chains (28). The differences in the intermolecular packing are reflected in the band ratio of I2885/I2850 and I2935/I2885 (28-32). The intensity of the ~2885 cm^{-1} band relative to ~2850 cm^{-1} decreases when the chains have fewer lateral interactions, as is the case when the chains are melted or dissolved. The I2885/I2850 ratio for the stable packings (β and β') of PP12 and PP14 varied between 1.8 to 1.6 and in the hexagonal packing (α-phase) this ratio is ~1.4. In PP14 the intensity ratio of I2885/I2850 (**Table 4**) of β'_2 and β'_1-phases (1.79 and 1.76) indicate greater lateral chain packing order than the β'_2, β'_1, and β-forms (1.67, 1.59, and 1.73) of PP12. This corroborates with the greater thermodynamic stability of β'_1-phase and the absence of β-phase in PP14 as discussed above. Bunow and Levin (32) observed that the ratio of I2935/I2885 decreases with the increasing lateral chain order of the phospholipid bilayers. In the stable O⊥ and T// packings of PP12 and PP14, this ratio is less than that of the hexagonal packing (Table 4). These observations confirm that the lateral chain order in the hexagonal phase is less than the orthorhombic and triclinic subcells. However, it is clear that the lateral chain packing order in the hexagonal subcell is much greater than the liquid (I2885/I2850 = ~0.80; I2935/I2885 = ~0.85).

In Raman spectrum the intensity ratios of the peaks in the C-C stretching region (1050-1150 cm^{-1}) provide a quantitative insight to the intrachain order of the hydrocarbon chains. The three bands that occur in this region are attributed to the *trans/gauche* content (9). The 1065 and 1130 are assigned to *trans* chain segments and the band near 1090 cm^{-1} is due to *gauche* conformation of the acyl chains. The intensity ratios I~1090/I1065 and I~1090/I1130 are directly proportional to *gauche/trans* content. The intrachain order of a phase can be assessed on the basis of these ratios. Table 4 shows these ratios in various polymorphic forms and in liquid of PP12 and PP14. In the three polymorphic forms the *gauche* content has increased in the order of $\alpha > \beta' > \beta$. However, the *gauche* content of hexagonal packing is much less than liquid and is comparable to O⊥ and T// packings. It supports the previous understanding of the hexagonal packing (1, 33) that there is no specific zig-zag plane orientation of the adjacent acyl chains with respect to each other, but the intrachain *trans* zig-zag conformation is largely maintained in this phase.

Packing along the long axis

The low-angle X-ray diffraction lines from all the phases of PP12 and PP14 are in the order of 39-45 Å. These long spacings correspond to a bilayer periodicity (two-chain-length structure) given the theoretical distances of 1.27 Å for the adjacent carbons of the acyl chain and 5.5 Å for the glycerol region. All the polymorphic forms of these two compounds are tilted; however, the tilt is greater in the more stable forms presumably to accomplish the optimal lateral chain packing. In all the phases the X-ray diffraction 001 order is more intense followed by 003 order. Wherever the 002 order is observed, it is the least intense. This intensity pattern is consistent with bilayer structure of other triacylglycerols observed by Sato et al. (34). We can expect that the orientation of the acyl chains in the bilayer would be similar to the trilaurin and tricaprin (11, 12) with the acyl chains at the 1- and 2-positions pointing in opposite directions; the acyl chain at the 3-position bends at the carbonyl region to lie parallel to the 1-acyl chain of the *sn*-glycerol.

The overall polymorphic behavior of PP12 and PP14 is shown in **Fig. 8**. For comparison, the polymorphic behavior patterns of the higher homologue, tripalmitoylglyc-

TABLE 4. Peak height ratios in the C-H and C-C stretching regions of the Raman spectrum of various phases of PP12 and PP14

Polymorph	Compound	I1090/I1065	I1090/I1130	I2885/I2850	I2935/I2885
β	PP12	0.20	0.19	1.73	0.26
β'_1	PP14	0.22	0.23	1.76	0.22
β'_1	PP12	0.22	0.23	1.59	0.28
β'_2	PP14	0.22	0.22	1.79	0.27
β'_2	PP12	0.26	0.25	1.67	0.29
α	PP14	0.28	0.25	1.41	0.30
α	PP12	0.27	0.26	1.43	0.30
Isotropic liquid	PP14	1.14[a]	1.22[a]	0.85	0.84
Isotropic liquid	PP12	1.16[a]	1.18[a]	0.80	0.88

[a]In the isotropic liquid the frequencies of 1066, 1100, and 1035 cm^{-1} moved to a lower frequency of approximately 1058, 1080, and 1018 cm^{-1}.

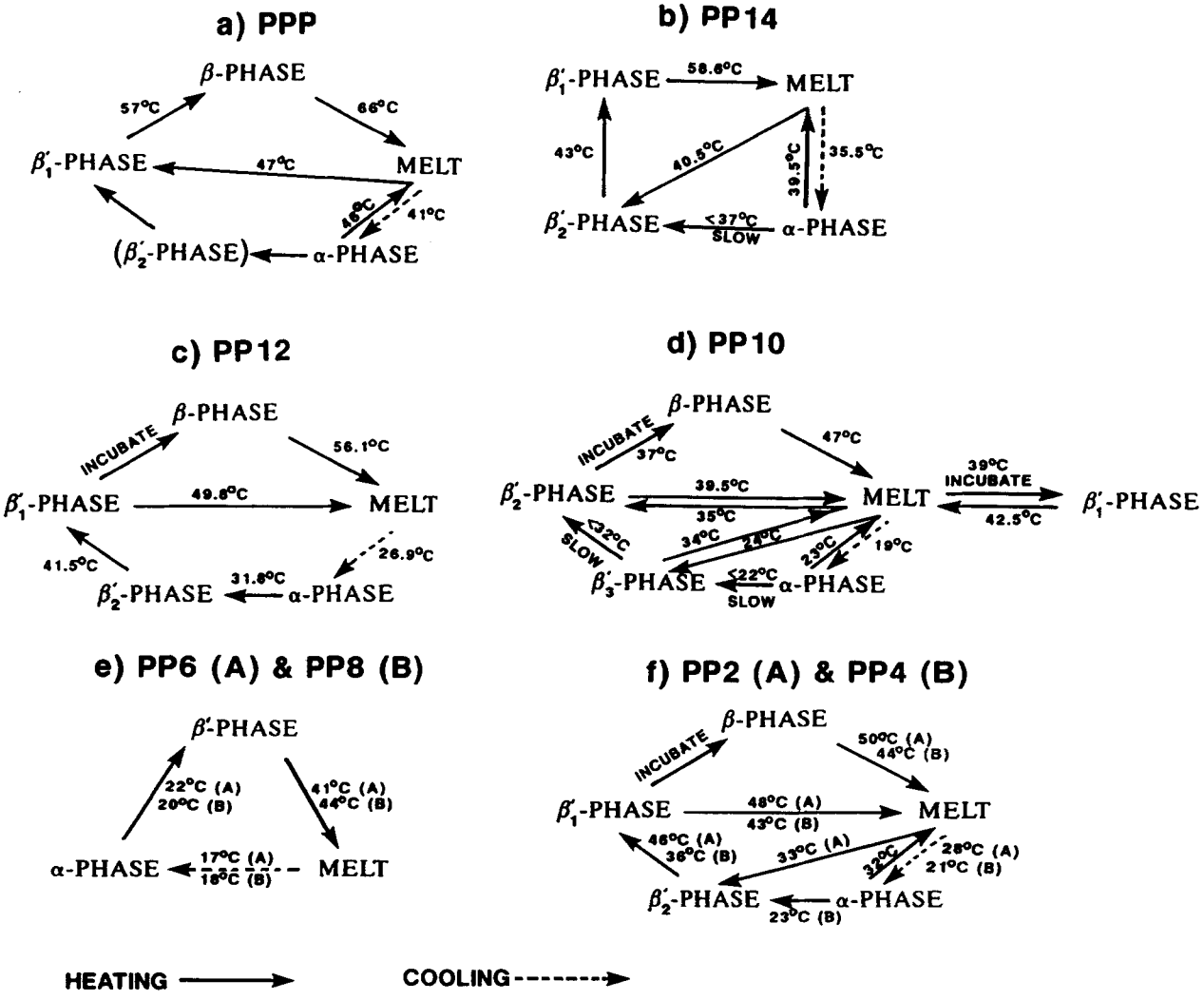

Fig. 8. The phase behavior of PP12 and PP14 compared to the higher and lower homologues of this series. The transformations of various phases are shown as arrows connecting one phase to another. The temperature of the transition is given over or under the arrow and dashed arrows indicate transitions obtained on cooling. For instance, the stable β'_1-phase of PP14 melts at 58.6°C. On cooling the melt undercools to 35.5°C where the α-phase nucleates and crystallizes. If the α-phase is allowed to stand below 37°C it will slowly transform to the β'_2-phase. However, if the α-phase is heated to its melting point (39.5°C), it rapidly converts to the β'_2-phase. The β'_2-phase will transform to the more stable β'_1-phase at 43°C.

erol (PPP) (22, 23) and the lower members of this series, 1,2-dipalmitoyl-3-acetyl (PP2), 3-butyryl (PP4), 3-hexanoyl (PP6), 3-octanoyl (PP8), and 3-decanoyl (PP10) (16, 17), are also schematically summarized in Fig. 8.

We thank David Jackson, Sridhar Dasari, and Balaji Bhiravabhatla for technical help, and Irene Miller and Anne Plunkett for typing the manuscript. The Raman spectra were recorded at MIT laser research center and biomedical research center (supported by NIH #RR02594 and NSF #CHE 8442185). This work is supported by the grant from NIH, HL-26335.

Manuscript received 22 March 1990 and in revised form 4 June 1990.

REFERENCES

1. Small, D. M. 1986. Glycerides. Chapter 10. *In* The Physical Chemistry of Lipids from Alkanes to Phospholipids. Plenum Press, New York. 345–372.
2. Small, D. M. 1984. Lateral chain packing in lipids and membranes. *J. Lipid Res.* **25:** 1490–1500.
3. Abrahamsson, S., B. Dahlen, H. Lofgren, and I. Pascher. 1978. Lateral packing of hydrocarbon chains. *Prog. Chem. Fats Other Lipids.* **16:** 125–143.
4. Chapman, D. 1962. The polymorphism of glycerides. *Chem. Rev.* **62:** 433–456.
5. Kobayashi, M. 1988. Vibrational spectroscopic aspects of polymorphism and phase transition of fats and fatty acids.

In Crystallization and Polymorhism of Fats and Fatty Acids. N. Garti and K. Sato, editors. Marcel Dekker Inc., New York. 139–187.
6. Fischmeister, I. 1974. Infrared absorption spectroscopy of normal and substituted long-chain fatty acids and esters in the solid state. *Prog. Chem. Fats and Other Lipids.* **24:** 91–162.
7. Snyder, R. G. 1961. Vibrational spectra of crystalline n-paraffins. II. Intermolecular effects. *J. Mol. Spectrosc.* **7:** 116–144.
8. Chapman, D. 1957. The 720 cm^{-1} band in the infrared spectra of crystalline long-chain compounds. *J. Chem. Soc.* 4489–4491.
9. Verma, S. P., and D. F. H. Wallach. 1984. Raman spectroscopy of lipids and biomembranes. *In* Biomembrane Structure and Function. D. Chapman, editor. Verlag Chemie, Weinheim. 167–199, and the references cited therein.
10. Bicknell-Brown, E., K. G. Brown, and W. B. Person. 1981. Configuration-dependent Raman bands of phospholipid surfaces. 2. Headgroup and acyl stretching modes in the 800–900 cm^{-1} region. *J. Raman Spectrosc.* **11:** 356–362.
11. Larsson, K. 1964. The crystal structure of the β-form of trilaurin. *Arkiv Kemi.* **23:** 1–15.
12. Jensen, L. H., and A. J. Mabis, 1966. Refinement of the structure of β-tricaprin. *Acta Crystallogr.* **21:** 770–781.
13. Fahey, D. A., D. M. Small, D. R. Kodali, D. Atkinson, and T. G. Redgrave. 1985. Structure and polymorphism of 1,2-dioleoyl-3-acyl-*sn*-glycerols. Three- and six-layered structures. *Biochemistry.* **24:** 3757–3764.
14. Kodali, D. R., D. Atkinson, T. G. Redgrave, and D. M. Small. 1987. Structure and polymorphism of 18-carbon fatty acyl triacylglycerols: effect of unsaturation and substitution in the 2-position. *J. Lipid Res.* **28:** 403–413.
15. Kodali, D. R., D. Atkinson, T. G. Redgrave, and D. M. Small. 1984. Synthesis and polymorphism of 1,2-dipalmitoyl-3-acyl-*sn*-glycerols. *J. Am. Oil Chem. Soc.* **61:** 1078–1084.
16. Kodali, D. R., D. Atkinson, and D. M. Small. 1989. Molecular packing of 1,2-dipalmitoyl-3-decanoyl-*sn*-glycerol (PP10): bilayer, trilayer and hexalayer structures. *J. Phys. Chem.* **93:** 4683–4691.
17. Kodali, D. R., D. Atkinson, and D. M. Small. 1989. Molecular packing in triacyl-*sn*-glycerols: influences of acyl chain length and unsaturation. *J. Dispersion Sci. Technol.* **10:** 393–440.
18. Larsson, K. 1966. Classification of glyceride crystal forms. *Acta Chem. Scand.* **20:** 2255–2260.
19. Franks, A. 1958. Some developments and applications of microfocus X-ray diffraction techniques. *Br. J. Appl. Phys.* **9:** 349–352.
20. Carter, M. G. R., and T. Malkin. 1939. An X-ray and thermal examination the glycerides. Part V: Unsymmetrical mixed triglycerides. *J. Chem. Soc.* 577–581.
21. Carter, M. G. R., and T. Malkin. 1939. An X-ray and thermal examination of the glycerides. Part VII: Unsymmetrical mixed triglycerides. *J. Chem. Soc.* 1518–1521.
22. Hagemann, J. W. 1988. Thermal behavior and polymorphism of acylglycerides. *In* Crystallization and Polymorphism of Fats and Fatty Acids. N. Garti and K. Sato, editors. Marcel Dekker Inc., New York. 9–95.
23. Ollivon, M. 1982. Ph. D. Thesis, à l'Université Pierre et Marie Curie, Paris.
24. Ollivon, M., and R. Perron. 1983. Phase transitions and polymorphism of saturated even monoacid triglycerides. Fat Science, Proceedings 16th ISF Congress, Budapest. 107–116.
25. Hernqvist, L. 1988. Crystal structures of fats and fatty acids. *In* Crystallization and Polymorphism of Fats and Fatty Acids. N. Garti and K. Sato, editors. Marcel Dekker Inc., New York. 97–137.
26. Simpson, T. D., and J. W. Hagemann. 1982. Evidence of two β'-phases in tristearin. *J. Am. Oil Chem Soc.* **59:** 169–171.
27. Bicknell-Brown, E., K. C. Brown, and W. B. Person, 1980. Configuration-dependent Raman bands of phospholipid surfaces. 1. Carbonyl stretching modes at the bilayer interface. *J. Am. Chem. Soc.* **102:** 5486–5491.
28. Larsson, K. 1973. Conformation-dependent features in the Raman spectra of simple lipids. *Chem. Phys. Lipids.* **10:** 165–176.
29. Gaber, B. P., and W. L. Peticolas. 1977. On the quantitative interpretation of biomembrane structure by Raman spectroscopy. *Biochim. Biophys. Acta.* **465:** 260–274.
30. Yellin, N., and I. W. Levin. 1977. Hydrocarbon chain disorder in lipid bilayers. Temperature-dependent Raman spectra of 1,2-diacylphosphatidylcholine-water gels. *Biochim. Biophys. Acta.* **489:** 177–190.
31. Yellin, N., and I. W. Levin. 1977. Hydrocarbon chain *trans-gauche* isomerization in phospholipid bilayer gel assemblies. *Biochemistry.* **16:** 642–647.
32. Bunow, M. R., and I. W. Levin. 1977. Comment on the carbon-hydrogen stretching region of vibrational Raman spectra of phospholipids. *Biochim. Biophys. Acta.* **487:** 388–394.
33. Snyder, R. G., M. Maroncelli, H. L. Strauss, C. A. Elliger, D. G. Cameron, H. L. Casal, and H. H. Mantsch. 1983. Distribution of *gauche* bonds in crystalline n-$C_{21}H_{44}$ in Phase II. *J. Am. Chem. Soc.* **105:** 133–134.
34. Sato, K., T. Arishima, Z. H. Wang, K. Ojima, N. Sagi, and H. Mori. 1989. Polymorphism of POP and SOS. I. Occurrence and polymorphic transformation. *J. Am. Oil Chem. Soc.* **66:** 664–674.